

Analysis of Microscale Transport for BioMEMS

C. D. Meinhart, M. Sigurdson & D. Tretheway

Department of Mechanical Engineering, University of California, Santa Barbara, CA 93106, USA

ABSTRACT

Micron-resolution Particle Image Velocimetry (micro-PIV) is used to measure fluid motion in 30 x 300 micron channels. The results indicate that the no-slip boundary condition may not necessarily hold for hydrophobic surfaces in micro and nanochannels. Micro-PIV is also used to measure AC electrokinetic flow. Microscale mixing can be induced by precisely controlled 20 micron vortices. Finite element simulations are used to show that these vortices can be used in Bio-MEMS to enhance receptor/ligand binding on functionalized surfaces by a factor of four to six.

SLIP FLOW BACKGROUND

At the macroscopic level, it is well accepted that the boundary condition for a viscous fluid at a solid wall is "no-slip", i.e. the fluid velocity matches the velocity of the solid boundary. While the no-slip boundary condition has been proven experimentally to be accurate for a number of macroscopic flows, it remains an assumption that is not based on physical principles. In fact, nearly two hundred years ago Navier (1823) proposed a general boundary condition that incorporates the possibility of fluid slip at a solid boundary. Navier's proposed boundary condition assumes that the velocity, u_w , at a solid surface is proportional to the shear stress at the surface

$$u_w = \beta \left. \frac{\partial u}{\partial y} \right|_{y=0}, \quad (1)$$

where β is the slip length or slip coefficient. If $\beta = 0$ then the generally assumed no-slip boundary condition is obtained. If β is finite, fluid slip occurs at the wall, but its effect depends upon the length scale of the flow. For example, the solution for Stokes flow between two infinite parallel plates separated by $2h$, with the boundary conditions of no shear stress at the centerline and Navier's hypothesis, Eq. (1), at the wall yields

$$u_w = -\frac{h^2}{2\mu} \left(\frac{dp}{dx} \right) \left[1 - \left(\frac{y}{h} \right)^2 + \frac{2\beta}{h} \right], \quad (2)$$

where μ is the viscosity, and dp/dx is the pressure gradient. The first two terms in the brackets, $1 - (y/h)^2$, is the standard parabolic solution for pressure-driven Stokes flow between two infinite parallel plates with no-slip, while the second term, $2\beta/h$, represents the uniform velocity profile associated with the slip boundary condition given by Eq. (1). The parabolic term is of order one while the second term depends upon the slip length, β , and the plate separation, h . Assuming that β is finite and constant, as h decreases the importance of the velocity slip term increases. Since the no-slip assumption appears to be valid at the

macroscale, β must be relatively small, on the order of microns or less. If β is of order one micron, then at the micro and nano length scales, which are associated with microfluidic devices, the velocity slip term can be significant and perhaps dominate Eq. (2).

Recently, several researchers have suggested that the well-accepted no-slip boundary condition may not be suitable at the micro- and nano-scales. With a hot-wire anemometer, Watanabe et. al. (1998, 1999) identify fluid slip at the wall of a strongly hydrophobic duct or pipe. Their velocity profiles are consistent with Navier's hypothesis. However, their results are for a relatively large-scale rectangular duct (15mm x 15mm) and modest Reynolds numbers.

Breuer et al. (2003) has very carefully performed experiments of flow rate verses pressure drop for atomically smooth microchannel surfaces. Their results indicate slip lengths on the order of ten's of nanometers for both hydrophobic and hydrophilic surfaces, with the hydrophobic surface slip length being larger. It is unclear whether the atomically smooth surfaces produce a smaller slip length, compared to surfaces with nano-scale roughness.

Ruckenstein and Rajora (1983) investigated fluid slip in glass capillaries with surfaces made repellent to the flowing liquid. Their experimental results of pressure drop indicate larger slip than that predicted by chemical potential theory, where slip is proportional to the gradient in the chemical potential. The results suggest that slip occurs over a gap near the surface rather than directly on the solid surface, and the gap forms when a hydrophobic liquid flows over a hydrophilic surface and vice versa. They suggest that the gap may be increased in thickness by the release of gases entrained in the flowing liquid and/or the desorption of soluble gases. Their results, however, are inferred from pressure drop-flow measurements and not direct measurement of the fluid velocities.

Computationally, Barrat and Bocquet (1999) expect significant slip in nanoporous medium when the liquid is sufficiently non-wetting, which increases the effective permeability of the nanoporous medium. Their predictions are experimentally justified by Churaev et. al. (1984). Churaev et al. (1984) postulated slip at the wall to recover the viscosity of water for water flow in thin ($<1 \mu\text{m}$) hydrophobic capillaries. Pit et. al. (2000) observed fluid slip for hexadecane between two rotating parallel disks with a gap of 190 microns. By following the movement of a photo-bleached test section, they measure no slip when the surfaces are coated with perfluorodecanetrichlorosilane, a slip length of approximately 170nm for bare sapphire, and a slip length of 400nm for an octadecyltrichlorosilane (OTS) coating. They conclude that slip depends on both the interfacial energy and surface roughness.

Zhu and Granick (2001) experimentally observe fluid slip in an oscillating surface force

apparatus. For cylinder separations from approximately 10-200nm, they measured slip lengths of up to 2.5 μm for water between octadecyltriethoxysilane (OTE) surfaces, 1.5 μm for tetradecane between OTE surfaces, and 0.9 μm for tetradecane between mica surfaces. Their results suggest a strong dependence between the velocity gradient and magnitude of the slip, a critical shear rate for onset of fluid slip, and an increase in the slip length as the separation between the cylinders decreases. Their conclusions, however, are inferred from discrepancies between the measured normal force and expected normal force assuming no-slip, and are not measured directly. More recently, Zhu and Granick (2002) examine the relative importance of surface roughness and fluid-surface interactions in determining the appropriate boundary condition. For similar, poorly wetting surfaces the critical shear rate to observe deviations from force predictions assuming no-slip increased nearly exponentially with increasing surface roughness. They conclude that local intermolecular interactions are dominant when surfaces are very smooth, but are otherwise negligible at sufficient surface roughness.

Tretheway and Meinhart (2002) measured fluid velocities in hydrophilic and hydrophobic microchannels by micron resolution particle image velocimetry (micro-PIV). Their results showed a significant fluid velocity near a hydrophobic microchannel wall and no-slip for a hydrophilic surface. A slip length of $\beta = 0.92 \mu\text{m}$ was estimated from the micro-PIV data.

SLIP FLOW PIV MEASUREMENTS

Micro-resolution PIV has been developed over the past six years, and is now a well-accepted tool for probing microfluidic devices (see Meinhart et al., 1999; Meinhart & Zhang, 2000; Stone et al., 2002; Meinhart & Wereley, 2003; Meinhart et al., 2003). Previously, we have examined the no-slip boundary condition by applying micron-resolution particle image velocimetry (μ -PIV) to measure the flow of water in microchannels that have a clean surface (hydrophilic) and in microchannels that are coated with hydrophobic octadecyltrichlorosilane (OTS). The initial direct measurements show fluid slip for water flowing over a solid hydrophobic surface and no-slip for a hydrophilic surface.

Figure 1 is a velocity field measured in the $30 \times 300 \mu\text{m}$ microchannel, with a clean hydrophilic surface. High spatial resolution velocity measurements are obtained by averaging 20 correlation functions at each interrogation spot. Near the wall, the interrogation spots are $13.8 \times 0.9 \times 1.8 \mu\text{m}$. By overlapping the interrogation spots by 50%, the spacing between velocity vectors is 450 nm, with the lowest measurement being within 450 nm of the wall. The measurements are taken in the mid-plane of the channel (15 μm from the bottom) near the side wall. The field of view is aligned such that a section of the wall is included in each image. Since there are no particles in the wall, the resulting correlations for that region produce erroneous velocity vectors with magnitudes and directions that are inconsistent with the known direction of flow. The wall location is then set at the point at which the velocity vectors are erroneous.

The uncertainty in determining the wall location by this method is approximately 450nm. From Fig. 1 it is clear that that no-slip boundary condition is valid for the hydrophilic $30 \times 300 \mu\text{m}$ microchannel.

The velocity data shown in Fig. 1 is averaged in the streamwise direction to obtain an average velocity profile. A similar microchannel was coated with a monolayer of OTS, to make the surface hydrophobic. The PIV experiment was repeated with the same flow conditions, except the surface is hydrophobic. Figure 2 shows the average velocity profile for flow near the wall for hydrophilic (squares) and hydrophobic (triangles) microchannel surfaces. The velocity profiles are normalized by the free-stream velocity.

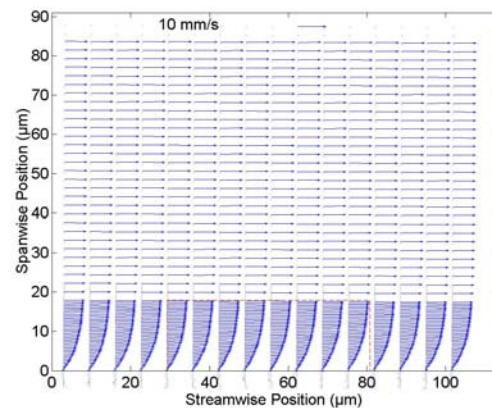


Figure 1. Velocity vector field of fluid moving through a $30 \times 300 \mu\text{m}$ microchannel with a hydrophilic surface. The spatial resolution is $0.9 \times 13.8 \times 1.8 \mu\text{m}$. Near the wall at $y = 0$, the velocity decreases to zero. The results indicate that the no-slip boundary condition appears to be valid for hydrophilic channels at this scale.

For a hydrophilic surface (squares), Fig. 2 shows the velocity approaching its free-stream value at 25 μm from the wall and smoothly decreasing to zero at the wall. This profile is consistent with the analytical solution for flow through a rectangular duct with a finite aspect ratio, assuming the no-slip boundary condition (White, 1974). For flow through a hydrophobic microchannel, the velocity profile is significantly different. While Fig. 2 shows the hydrophobic velocity profile (triangles) near its free-stream value at 25 μm and decreasing towards the wall, a finite and significant velocity is measured within 450 nm above the wall. This slip velocity is approximately 9% of the free-stream velocity, and effectively shifts the entire velocity profile when compared with the no-slip profile (squares). As a result, the velocity 25 μm from the wall in a hydrophobic microchannel is approximately 95% of the free-stream velocity, compared with 90% for a microchannel that is hydrophilic. Thus, a monolayer of hydrophobic molecules with a thickness of less than 2.3 nm significantly affects the velocity profile, even out to a distance of 25 μm from the wall. The observed shift in the velocity profile is consistent with the results of Watanabe et al. (1998, 1999), even though their results are for a flow through a significantly larger duct and at higher Reynolds number.

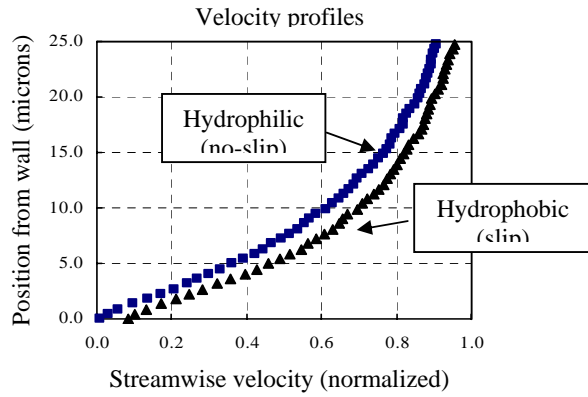


Figure 2. Velocity profiles for flow over a hydrophilic (square) and hydrophobic (triangle) microchannel surface. The velocity profiles are normalized by the free-stream velocity.

AC ELECTROKINETICS

AC electrokinetics refers to induced particle or fluid motion resulting from externally applied AC electric fields. While DC electrokinetics has been widely used for lab-on-a-chip applications such as electroosmotic pumping (Chien, 02; Bousse, 00), and capillary gel electrophoresis for DNA fractionation (Thormann, 01), AC electrokinetics has not been exploited in detail.

AC electrokinetics are advantageous over DC electrokinetics because they minimize electrolysis, and operate at lower voltages (1~20 V). AC electrokinetics can be classified into three broad areas: dielectrophoresis (DEP), electrothermal forces and AC electro-osmosis (Ramos *et al.*, 1998).

Dielectrophoresis is a force arising from differences in polarizability between the particle and the fluid medium in the presence of a non-uniform electric field. DEP has been used to separate blood cells and to capture DNA molecules (Miles *et al.*, 1999; Wang *et al.* 1998; Washizu *et al.*, 1995; & Yang *et al.*, 1999; Gascoyne, 2002). However, since the force scales with the cube of particle radius, it is ineffective for manipulating nanoscale molecules (such as 10nm-scale antigens).

AC electroosmosis arises when the tangential component of the electric field interacts with a field-induced double layer along a surface. It becomes less important above a certain electric field frequency. For example, in an aqueous saline solution with an electrical conductivity of $\sigma = 2 \times 10^{-3}$ S/m, it is predicted that AC electroosmosis is not important above 100 kHz (Ramos, 02).

Transport enhancement for small proteins may be most successful through electrothermally-driven flow (ETF). A non-uniform electric field produces uneven Joule heating of the fluid, which gives rise to nonuniformities in conductivity and permittivity. These interact with the electric field to generate flow. Characteristic swirling flow patterns can be used to circulate suspended molecules past the binding region, thereby providing more binding opportunity for the suspended molecules.

ELECTROTHERMAL SIMULATIONS

The finite element solver *Femlab* (developed by *Comsol*, Stockholm, Sweden) is used to simulate electrothermally-induced flow and subsequent enhanced binding in the cavity. First, the two-dimensional quasi-static potential field for two stripe electrodes along the cavity wall is calculated, according to Laplace's Equation, $\nabla^2 V = 0$. The resulting electric field, given by $\vec{E} = -\nabla V$ gives rise to a non-uniform temperature field through Joule heating. Ignoring unsteady effects and convection, and balancing thermal diffusion with Joule heating yields

$$k\nabla^2 T + \sigma E^2 = 0, \quad (3)$$

where T is temperature, E the magnitude of the electric field, and k and σ are the thermal and electrical conductivities. The resulting temperature field is shown in Fig. 3a. Boundary conditions are insulating except at the metal electrodes, which are isothermal at the ambient temperature. At the microchannel inlet and outlet, the Robin boundary conditions are applied to model the convective flux, which would result from the microchannel being at ambient temperature a distance of 1 mm from the sensing region. Convective flux at the inlet and outlet is negligible.

Gradients in temperature produce gradients in permittivity and conductivity in the fluid. For water ($1/\sigma$) $(\partial\sigma/\partial T) = +2\%$ and $(1/\epsilon) (\partial\epsilon/\partial T) = -0.4\%$ per degree Kelvin. These variations in electric properties produce gradients in charge density and perturb the electric field. Assuming the perturbed electric field is much smaller than the applied electric field, and that advection of electric charge is small compared to conduction, the time-averaged electrothermal force per unit volume for a non-dispersive fluid can be written as (Ramos *et al.*, 1998)

$$\vec{F}_{ET} = -0.5 \left[\left(\frac{\nabla\sigma}{\sigma} - \frac{\nabla\epsilon}{\epsilon} \right) \vec{E}_{rms} - \frac{\epsilon \vec{E}_{rms}}{1 + (\omega\tau)^2} + 0.5 |\vec{E}_{rms}|^2 \nabla\epsilon \right] \quad (4)$$

where $\tau = \epsilon/\sigma$ is the charge relaxation time of the fluid medium. The temperature-dependent variations in the electrical properties are written as

$$\nabla\epsilon = \left(\frac{\partial\epsilon}{\partial T} \right) \nabla T, \quad \nabla\sigma = \left(\frac{\partial\sigma}{\partial T} \right) \nabla T \quad (5)$$

The first term on the right hand side of Eq. (4) is the Coulomb force, and is dominant at low frequencies. The second term is the dielectric force, and is dominant at high frequencies. The crossover frequency scales inversely with the charge relaxation time of the fluid; an aqueous solution with conductivity 10^{-2} S/m has a crossover frequency around 14 MHz.

The electrothermal force shown in Eq. (4) is a body force on the fluid. The motion of the fluid can be determined by solving the Stokes' equation for zero Reynolds number fluid flow, such that

$$0 = -\nabla P + \mu \nabla^2 \vec{u} + \vec{F}_{ET}, \quad (6)$$

where \vec{u} is the fluid velocity, P is the pressure in the fluid, and μ is the dynamic viscosity of the fluid. Figure 3b shows the resulting velocity field. The velocity of the ETF is of order 400 $\mu\text{m/s}$, and characterized by a pair of counter rotating vortices, which may effectively circulate the analyte. If antibodies have been immobilized on the channel wall in a region of increased flow, these eddy motions will transport antigen to the antibody binding region.

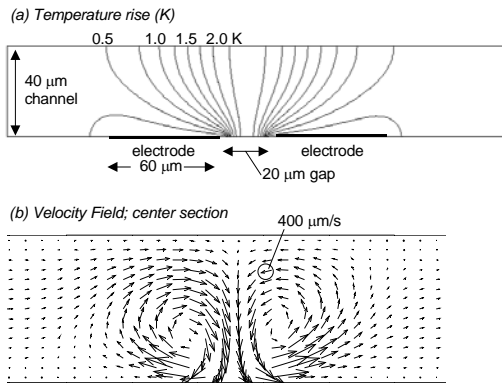


Figure 3. Simulation of electrothermally-driven flow in a 40 μm channel using Femlab software. (a) Non-uniform temperature distribution created by Joule heating, and (b) Electrothermally-driven fluid motion. The velocity of the electrothermally-driven flow is of order 400 $\mu\text{m/s}$ and is characterized by a pair of counter rotating vortices

The convective-diffusion equation is solved in combination with a first order reaction kinetic equation at the surface. The velocity field produced by the electrothermally-driven flow is used to mix antigen, thereby enhancing transport in a diffusion-limited reaction. The binding rates for 0, 7 and 14 Volts rms are shown in Fig. 4. As indicated by Fig. 4, the binding rate is increased by a factor of 6.5 for an applied voltage of 14 Vrms.

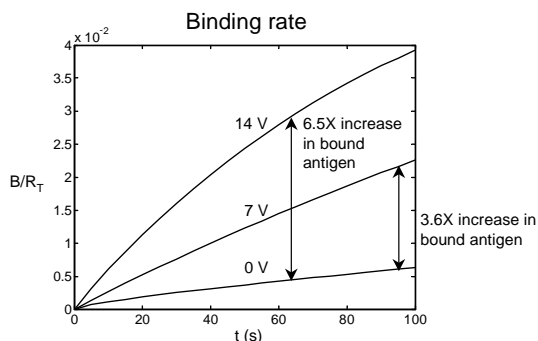


Figure 4 Binding curves for non-enhanced (0 V) and enhanced (7V & 14V) transport. The differences in the two curves show an increase in binding rate which yields a factor of 3.6 higher binding for 7 V and a factor of 6.5 higher binding for 14 V.

CONCLUSIONS

Micron-resolution Particle Image Velocimetry has been used to measure fluid velocity in 30 x 300 micron channels. When the surface chemistry is hydrophilic, the no-slip boundary condition is observed. However, when the surface is hydrophobic, a slip length of 0.9 μm is observed. This is consistent with measurements of Zhu & Granick (2001, 2002).

Numerical simulations of AC electrokinetic flow indicate that electrothermal phenomena can be used for localized micro-stirring. The stirring can be used to enhance the transport of molecules to a functionalized surface, thereby enhancing binding rates. With an applied voltage of 14 Vrms, the binding rate is increased by a factor of six.

REFERENCES

- Barrat, J and L. Bocquet, (1999) "Large slip effect at a nonwetting fluid-solid interface". *Phys. Rev. Lett.*, **82**, 4671.
- Bousse L. Cohen C. Nikiforov T. Chow A. Kopf-Sill AR. Dubrow R. Parce JW. Electrokinetically controlled microfluidic analysis systems [Review]. *Annual Review of Biophysics & Biomolecular Structure*. 29:155-181, 2000.
- Breuer, K. (2003) Personal Communication.
- Chien, Ring-Ling et al., Simultaneous hydrodynamic and electrokinetic flow control, *Micro Total Analysis Systems 2002, Volume 1*, 386-388, November, 2002.
- Churaev, N., V. Sobolev, and A. Somov, (1984) "Slippage of liquids over lyophobic solid surfaces". *J. of Colloid and Interface Science*, **97**, 574.
- Gascoyne PRC. Vykoukal J. Particle separation by dielectrophoresis [Review]. *Electrophoresis*. 23(13):1973-1983, 2002 Jul.
- Meinhart, C. D., D. Wang & K. Turner (2002) Measurement of Ac Electrokinetic Flows. Accepted *J. Biomedical Microdevices*.
- Meinhart, C. D., & S. T. Wereley (2002) Micron Resolution Particle Image Velocimetry, in *Diagnostic Techniques for Microfluidics*, Kenny Breuer Ed., Springer-Verlag, Berlin, in press.
- Meinhart, C. D. and H.S. Zhang (2000) The flow structure inside a microfabricated inkjet printhead. *Journal of MEMS* **9**, (no.1) IEEE March 2000, pp. 67-75.
- Meinhart, C. D., S. T. Wereley, and J. G. Santiago (1999) Micron-Resolution Velocimetry Techniques. In *Developments in Laser Techniques and Applications to Fluid Mechanics*, R. J. Adrian et al. (Eds.), Springer-Verlag, Berlin
- Miles, R., P. Belgrader, K. Bettencourt, J. Hamilton, S. Nasarabadi, 1999. Dielectrophoretic manipulation of particles for use in microfluidic devices, *MEMS-Vol. 1, Microelectromechanical Systems (MEMS), Proceedings of the ASME International Mechanical Engineering Congress and Exposition*, Nashville, TN, Nov. 14 – 19.
- Navier, C. L. M. H, (1823) *Memoirs de l'Academie Royale des Sciences de l'Institut de France*, **1**, 414.

- Pit, R., H. Hervet, and L. Leger, (2000) "Direct experimental evidence of slip in hexadecane: solid interfaces". *Phys. Rev. Lett.*, **85**, 980.
- Ramos, A., A. Castellanos, A. Gonzales, H. Morgan, N. Green. Manipulation of Bio-Particles in Microelectrode Structures by means of Non-Uniform AC Electric Fields. *Proceedings of ASME International Mechanical Engineering Congress & Exposition* Nov. 17-22, 2002, New Orleans, LA.
- Ramos, A., H. Morgan, N.G. Green and A. Castellanos, 1998. AC electrokinetics: a review of forces in microelectrode structures. *J. Phys. D: Appl. Phys.* **31**, 2338–2353.
- Ruckenstein, E. and P. Rajora (1983) "On the no-slip boundary condition of hydrodynamics". *J. of Coll. and Interface Sci.*, **96**, 488.
- Stone, S. W., C. D. Meinhart, & S. T. Wereley (2002) A Microfluidic-based nanoscope. In Press *Exp in Fluids*.
- Thormann, W., I. Lurie, B. McCord, U. Mareti, B. Cenni, N. Malik. Advances of capillary electrophoresis in clinical and forensic analysis (1999–2000). *Electrophoresis 2001*, **22**, 4216-4243.
- Tretheway, D. and C. Meinhart (2002) "Apparent Fluid Slip at Hydrophobic Microchannel Walls". *Phys. of Fluids*, **14**, L9-L12.
- Wang, X-B, Vykoukal, J., Becker, F. & Gascoyne, P. 1998. Separation of polystyrene microbeads using dielectrophoretic/gravitational field-flow-fractionation. *Biophysical Journal*, Vol. 74, pp. 2689-2701.
- Washizu, M., O. Kurosawa, I. Arai, S. Suzuki, N. Shimamoto, 1995 Applications of electrostatic stretch and positioning of DNA, *IEEE Transactions on Industry Applications*, Vol. 32, No. 3, pp. 447-445.
- Watanabe, K., Yanuar, and H. Mizunuma, (1998) "Slip of newtonian fluids at solid boundary". *JSME International Journal Series B*, **41**, 525.
- Watanabe, K., Yanuar, and H. Udagawa, (1999) "Drag reduction of newtonian fluid in a circular pipe with a highly water-repellant wall". *J. of Fluid Mech.*, **381**, 225.
- White, F. (1974) *Viscous Fluid Flow*, McGraw-Hill Publishing Co., New York, New York, 123.
- Yang, J. Huang, Y., Wang, X., Wang, X-B, Becker, F. Gascoyne, P. 1999. Dielectric properties of human leukocyte subpopulations determined by electrorotation as a cell separation criterion. *Biophysical Journal*, Vol. 76, pp. 3307-3314.
- Zhu, Y. and S. Granick, (2001), "Rate-dependent slip of Newtonian fluids at smooth surfaces". *Phys. Rev. Lett.* **87**, 96 (2001).
- Zhu, Y. and S. Granick (2002) "Limits of the Hydrodynamic No-Slip Boundary Condition" *Phys. Rev. Lett.* **88**, 106102.